Chapter 11

THE THERMAL RADIATION BALANCE EXPERIMENT ON BOARD EXPLORER VII

Dr. V. E. Suomi
University of Wisconsin
Madison, Wisconsin

SECTION I. INTRODUCTION

The value of the sun's radiant energy at the mean distance of the earth's orbit is 2.00 calories per square cm per minute. Since the earth intercepts the sun's radiation as a disk and reradiates it as a sphere, were the earth a perfect absorber the average loss per square cm at equilibrium would be one fourth the solar constant or 0.5 calories per cm squared per minute. The earth's surface is not a perfect absorber and in addition it is covered with an atmosphere. Part of the solar energy is reflected by Raleigh scattering in the atmosphere. We see this as the blue sky. Clouds exercise the most important variable control on the amount of sunshine the earth absorbs for they act as highly reflecting shutters. A small part of the sunlight is absorbed by the gases in the atmosphere, principally water vapor and ozone. Still another small fraction is absorbed by clouds, dust and smoke. By and large, however, most of that which is not reflected passes through the atmosphere to the earth's surface. The amount absorbed per unit area of the earth's surface depends on the sun's zenith angle and the surface properties. The oceans, for example, absorb most of it, about 95%, while polar snow fields absorb much less, about 10%. There are land surfaces which range between these extreme values. Reflected solar radiation is lost to space and never enters into the global thermodynamic system. The remaining solar energy is absorbed mainly at the earth's surface so it acts like the boiler lining of the giant heat engine which drives the atmosphere. The solar input to each unit area of the earth's surface depends on the latitude, time of year, and state of the atmosphere above. The effects of latitude and season on the incoming solar energy are well known; however, the effects of the atmosphere, especially over large parts of the earth where weather observations are unavailable, are only estimates.

Our understanding of the global distribution of long wave energy lost to space is even less well-known. Water vapor, carbon dioxide, ozone and other minor gases in the atmosphere selectively absorb the long wave energy radiated from the earth's surface and other layers of

the atmosphere to act as a very complex greenhouse effect. The long wave loss from the top of the atmosphere is three to four times as great as the net long wave loss at the earth's surface. This makes the atmosphere act as the principal heat sink whereas the earth's surface is the main heat source. It is possible to calculate the long wave heat loss from the atmosphere when the vertical distribution of temperature and infrared radiation absorbers are known, and these calculations have been carried out by Simpson, Bauer and Phillips, Houghton and more recently by London. These calculations are handicapped by lack of complete data on the vertical distributions of temperature and absorbers on a global basis and particularly on the lack of adequate middle and upper cloudiness data. Meteorologists have up to now been limited to viewing clouds from the bottom up rather than from the outside of the atmosphere down towards the earth. Despite the observational shortcomings, these studies have clearly shown that parts of the earth are in radiation imbalance. The tropics receive more energy from the sun than they lose by long wave radiation to space. Conversely the polar regions lose more energy to space by long wave radiation than they gain energy from the sun. Since on the average the tropics are not warming and the polar regions are not cooling the excess and deficit is made up by the poleward transport of heat by the atmosphere and the ocean currents. This poleward heat transport is the fundamental cause of the world's weather.

These studies assumed that the earth is in radiational equilibrium with space. That is, the total heat gain from the sun is just balanced by the loss to space. This assumption cannot be accepted without qualification for periods considerably in excess of a year or even tens of years for to do so would be to imply no climatic change. The atmosphere does not have a large heat capacity to smooth out the temporal imbalances. Rossby states that a change, for example, of only 1% in the incoming solar energy, would if applied only to the atmosphere cause a world wide air temperature change of six degrees Centigrade. The oceans have a much greater ability to store or provide the excess or deficit. A one percent change in the annual heat budget would change the ocean temperature only a few tenths of a degree if confined to the surface layers and might only be a few thousandths of a degree depending on the depth of the layer affected. A fundamental question concerning the heat balance of the earth is, "Is there a self regulating mechanism?" We might expect, for example, that an increase in net global energy might cause more evaporation from the oceans which cause more clouds to give less solar input to give less evaporation to cause fewer clouds resulting in more solar input, etc. The experiment on board Explorer VII cannot provide the answer for this question. We do not obtain observations from the whole earth and the orbit is not the best for this purpose; nevertheless we can expect a significant increase in the trustworthiness of the observations over what we have had up to now.

SECTION II. INSTRUMENTATION SYSTEM AND SENSORS

The instrumentation system, Figure 124, will now be described in more detail with particular emphasis on those portions which may be considered contributions to the art because of function, small size, low power consumption, etc.

1. Sensors

The sensors in all cases are variable resistance elements for measurement of temperature or erosion. All temperature sensing elements are thermistors.

Three radiation currents are measured with simple bolometers in the form of hollow silver hemispheres. The hemispheres are thermally isolated from but in close proximity to specially aluminized mirrors. The image of the hemisphere which appears in the mirror makes the sensor look like a full sphere. The mirror is made large enough so that no part of the hemisphere bolometer "sees" the satellite itself. The aluminum mirror surface has been evaporated following the procedure described by Hass, Bradford and Cox which gives the mirror a high reflectance in the ultraviolet portion of the solar spectrum. The mirror backed bolometers are mounted on the equator of the satellite. The temperature of the thin silver hemispherical bolometers is measured by a glass coated bead thermistor mounted so as to have good thermal contact to the hemisphere. In addition, provision is made to measure the temperature of the mirrors as well. This information is needed to account for any heat lost by conduction through the Kel-F hemisphere mounting posts. Figure 125 is a drawing illustrating the bolometer construction.

It is possible to show that a mirror backed hemisphere, by virtue of the satellite spin, acts as far as the radiation currents are concerned very similarly to an isolated sphere in space. Two of the hemispheres are provided with a black coating which makes them respond about equally to solar and terrestrial radiation. Another hemisphere is coated white. It is more sensitive to terrestrial radiation than to solar radiation. A fourth has a gold metal surface which makes it more sensitive to solar radiation than to terrestrial radiation. A black sphere is mounted on the axis of the satellite at the top. It is used to determine any deterioration in the mirror surfaces by comparison with the blackened hemispheres. Finally a small Tabor-surfaced hemisphere equipped with a shade to protect it from direct sunlight can be used to measure reflected sunlight when the axis of the satellite points to the earth's surface. The information telemetered to the earth's surface is the sensor temperatures. The radiation currents are obtained by using these temperatures in heat balance equations.

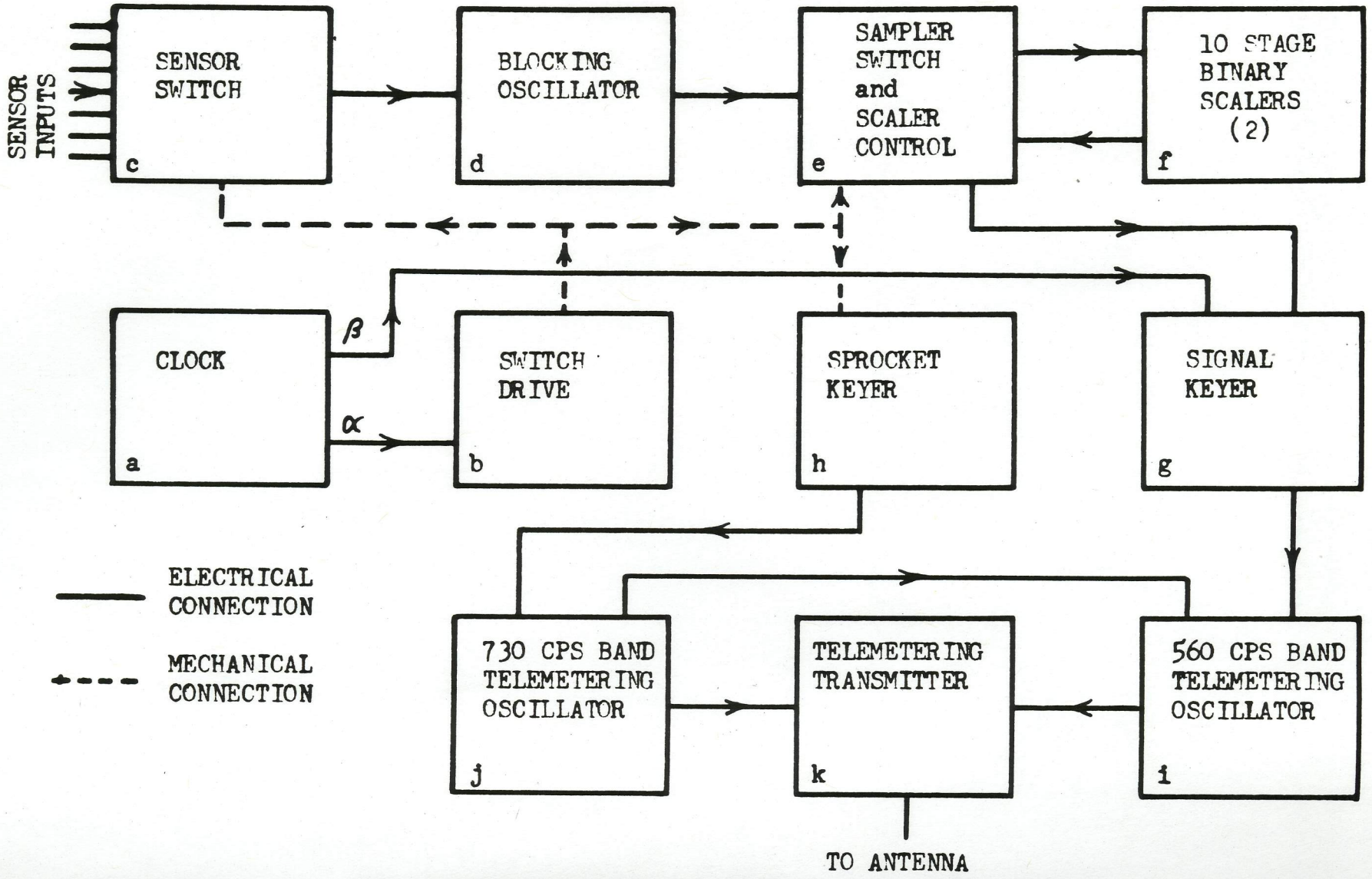

FIG. 124. BLOCK DIAGRAM OF UNIVERSITY OF WISCONSIN SYSTEM

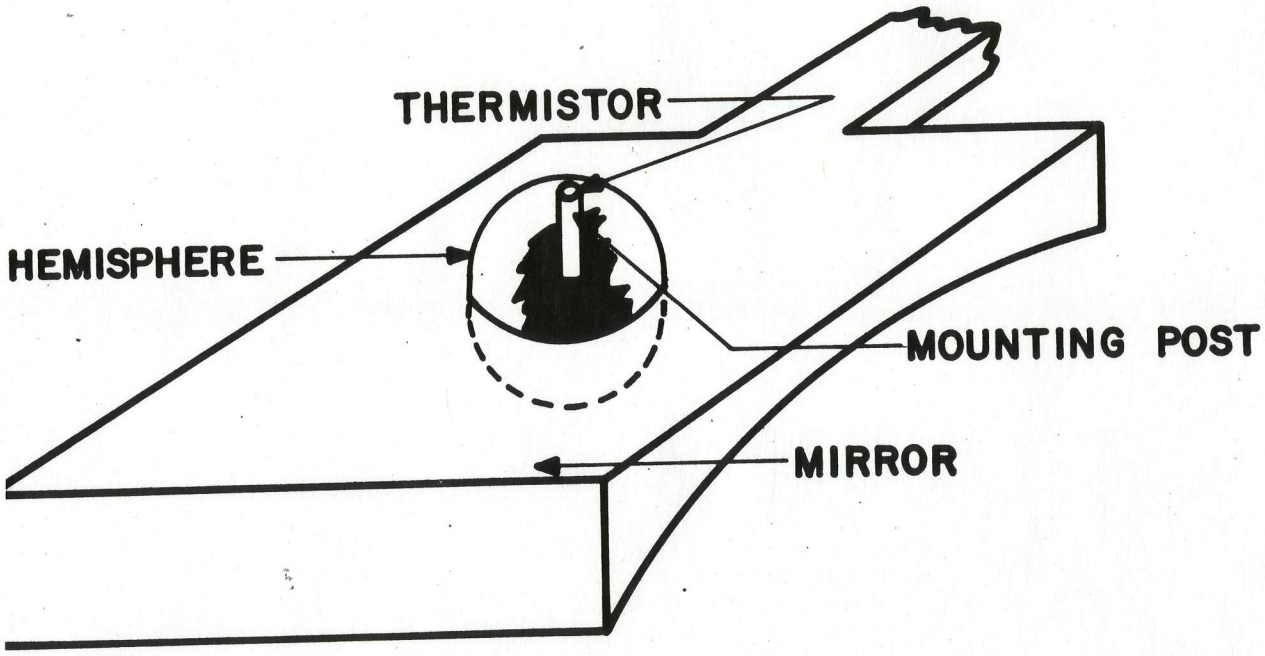

FIG. 125. BOLOMETER CONSTRUCTION

2. Sensor Commutator

All of the sensors operate continuously but the data from them are obtained by sampling, using time division multiplexing. The multiplexing is accomplished by a commutator switch driven by a Ledex solenoid. The drive for the solenoid is obtained from an electronic clock to be discussed later.

This system has provision for sampling 16 sensors. The sensors are not all sampled at the same rate. In this system as shown in Figure 126, there are seven segments on S_1 and nine segments on S_4. The wiper of S_1 remains on a segment for six seconds.

3. Blocking Oscillator

The sensor resistors are connected in turn by S_1 into the base circuit of a transistor blocking oscillator shown in Figure 127a to control its frequency of operation. The blocking oscillator thus performs the function of converting the resistance of the sensor to a corresponding frequency. The frequency of oscillation of the blocking oscillator is a linear function of the inverse of the resistance in its base timing circuit over a wide range, as shown in Figure 127b. The equation for frequency of oscillation is derived from the base waveform illustrated in Figure 127c.

$$(1) \qquad f = \frac{1}{\Gamma + KR} = \frac{-1}{KR} \qquad \text{for} \quad \Gamma \ll KR$$

where Γ = duration of the blocking oscillator pulse
K = a constant which includes C
R = total series base circuit resistance.

For the circuit constructed, $\Gamma = 50\ \mu$ - sec, and so for frequencies of oscillation up to 200 cps (period 5000 μ - sec) the error or departure from $F = 1/KR$ straight line relation is less than 1%. The form of the departure is illustrated by the dotted line in Figure 127b.

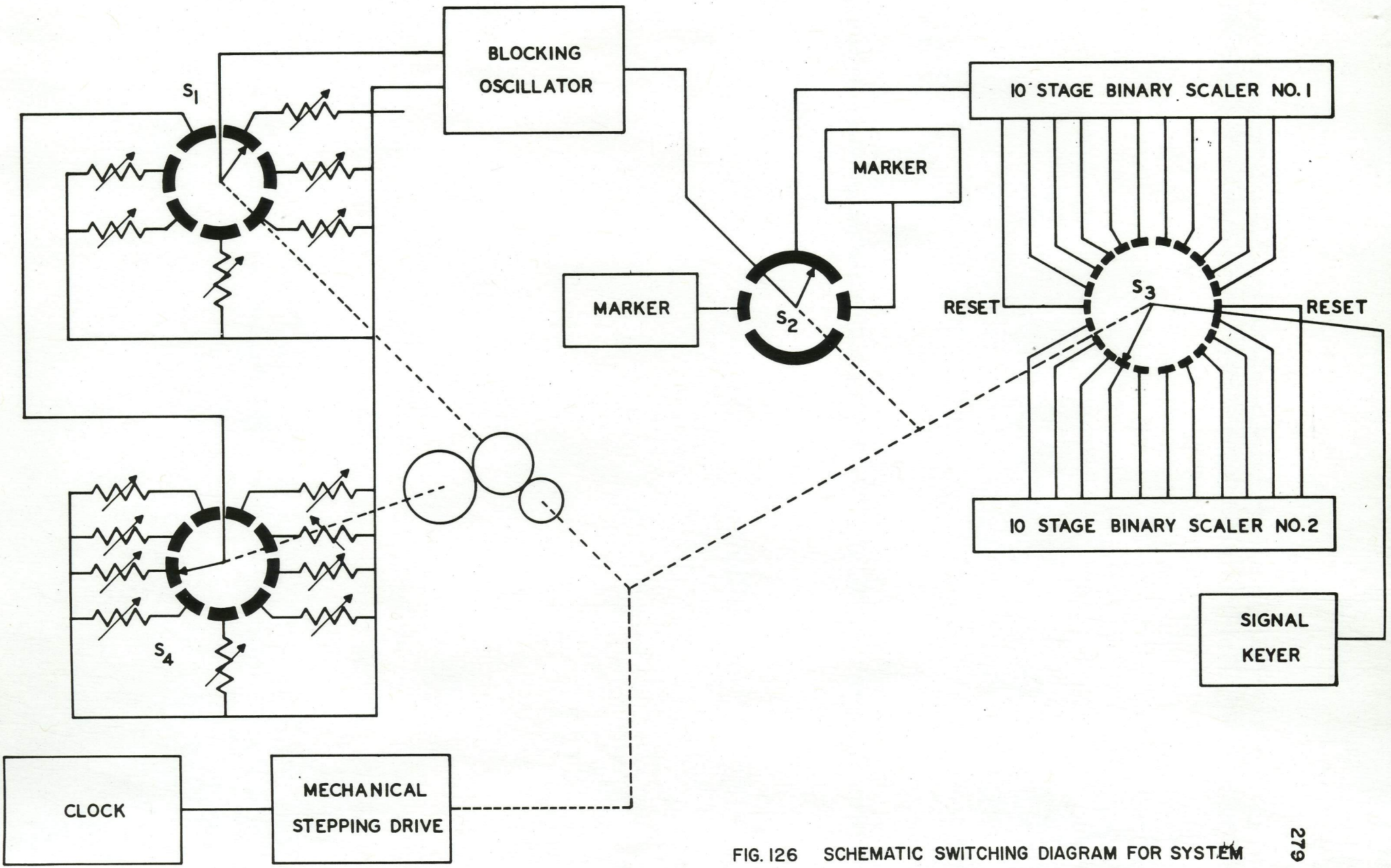

FIG. 126 SCHEMATIC SWITCHING DIAGRAM FOR SYSTEM

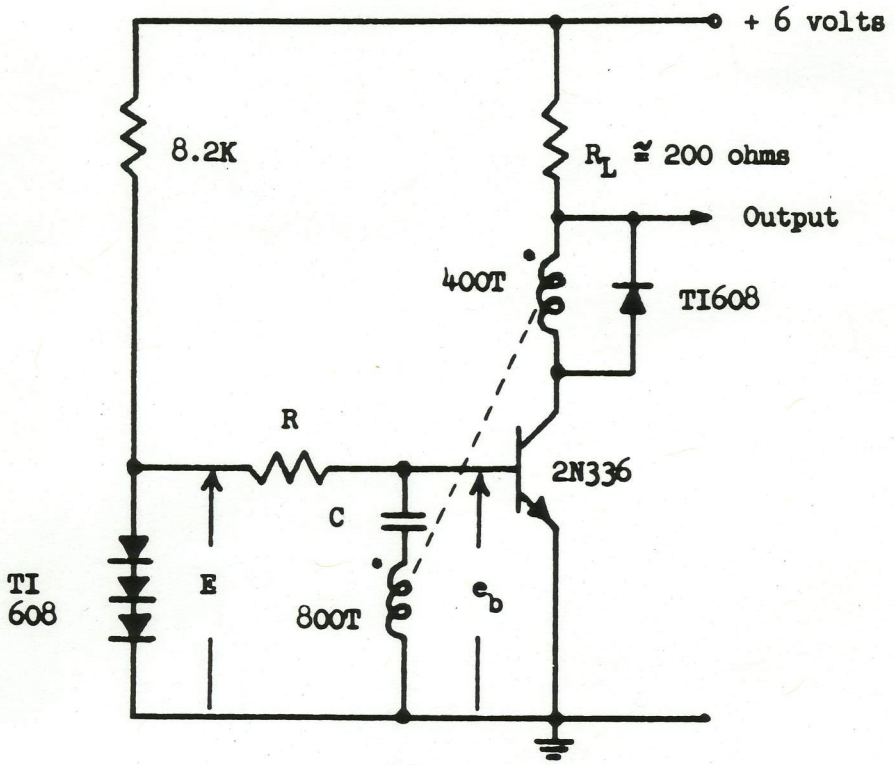

(a)

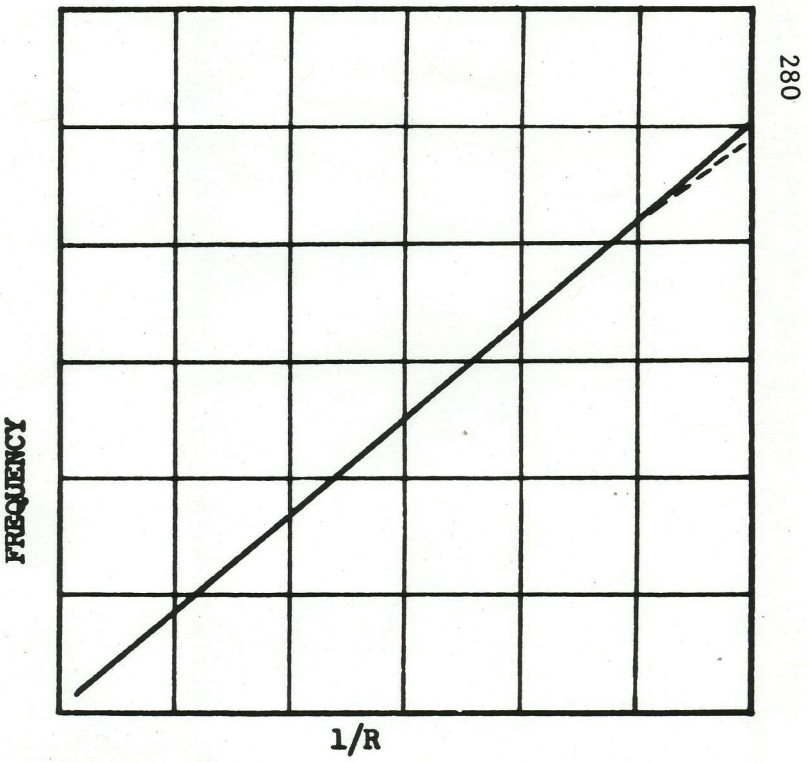

(b)

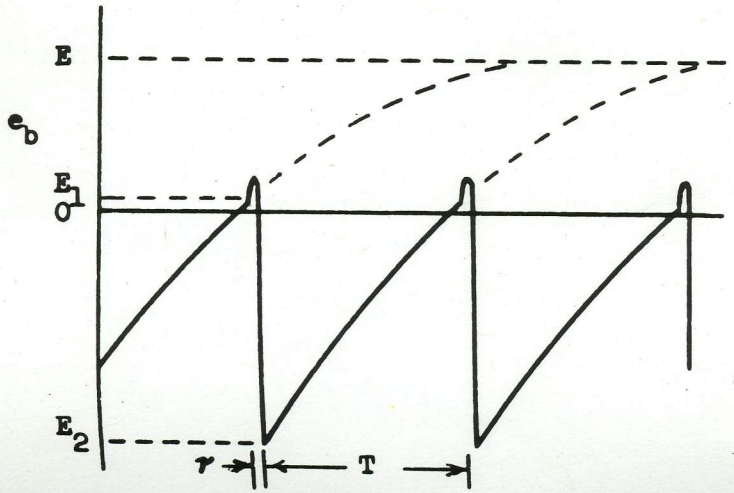

(c)

$$T = RC \ln \frac{E - E_2}{E - E_1} = KRC$$

$$f = \frac{1}{T + \tau} = \frac{1}{KRC + \tau}$$

$$\cong \frac{1}{KCR} \quad \text{for } \tau << KCR$$

There were a number of requirements on the blocking oscillator for this application:

a. To prevent heating and temperature measurement errors in the thermistors, the base circuit current had to be held to a few tens of microamperes.

b. High stability of frequency was necessary for rather wide ranges of temperature and supply voltage.

c. Low power consumption was required.

d. Linearity of f versus 1/R was necessary over a wide range of R. All of the above requirements were met without the use of temperature compensation, except for temperature effects of reference diodes, by careful selection of circuit elements and testing of circuit for stability of frequency versus temperature and supply voltage.

In order to maintain small values of base circuit charging current and hence thermistor current, silicon transistors of high beta and very low base leakage were selected. Low base leakage is particularly important for satisfactory operation with high values of R. The circuits developed oscillated satisfactorily with R as high as 10 megohms.

Temperature effects were overcome by using silicon transistors and by using the temperature compensating effects of the diodes which determine the reference potential to which R is returned.

The most critical single circuit element was found to be the collector resistor. It was found that proper selection of this resistor by experiment resulted in a circuit having minimum sensitivity to supply voltage changes.

Use of a saturating transformer resulted in close control of pulse width Γ over the range of operation and eliminated effects of Γ variations. Still more important, however, was its effect in standardizing the energy transfer to the base circuit each cycle and hence, the timing wave starting voltage E_2 of Figure 127c. A small value of Γ consistent with other considerations results in a lower duty cycle and hence lower power consumption. The blocking oscillator circuit appears to be unique because its duty cycle is much lower than that of other frequency generating circuits which might have been used.

With the design precautions described above, it was possible to construct a blocking oscillator having a frequency stability within two percent over a temperature range of -10^{o} to $65^{o}C$, and = 15% in supply voltage. With this small range in frequency over the temperature and supply voltage range above, and the straight line relation between f and 1/R, it is possible to make a linear correction for any condition and value of R which is a precision calibration resistor used in the system in at least one of the sensor positions. Actually, two precision calibrating resistors are used, one giving the normal maximum expected frequency and the other giving a frequency near the minimum expected. These calibrating resistors then allow correction of frequency to standard conditions. In addition, if drifts due to aging or other effects take place, it is possible to correct such effects by calculation referenced to the frequency corresponding to the calibrating resistors. The calibration with the resistor yielding the high frequency gives a sensitive measure of deviation from standard conditions while the calibration with the resistor yielding the low frequency (1.0 megohm in this case) gives a check on the leakage current of the transistor or in the associated circuits which may increase due to aging or other effects.

4. Binary Scalers

The ten stage binary scalers perform three functions: to count the output pulses from the blocking oscillator during a five-second interval, to form a ten-digit binary number representing the count of blocking oscillator pulses, and to store this number until readout.

The requirements on the binary scalers were as follows:

a. Reliability

b. Low power consumption

c. Capability of being reset

d. Operation over wide temperature and moderate supply voltage ranges

e. Counting rate up to at least two kilocycles per second

f. Capability of being sampled for readout.

All of the requirements were met by the circuit of Figure 128. The binary scaler is made up of ten such stages in cascade. The scaler stages are of more or less conventional design. However, to meet the power consumption limits it was necessary to design the circuit at a high impedance level. Each stage requires approximately 600 microwatts

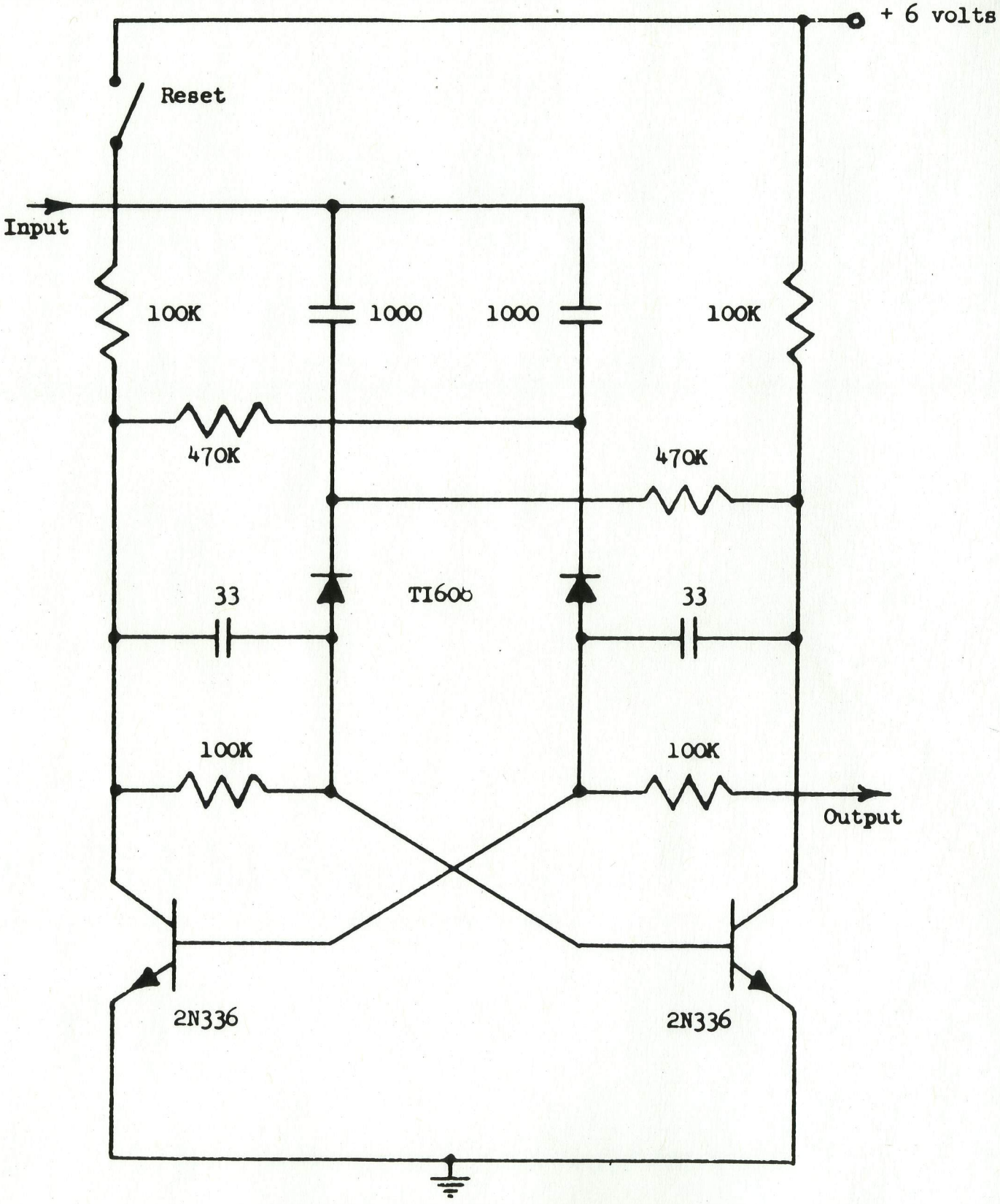

FIG. 128. BINARY SCALER CIRCUIT

with the ten-stage scaler thus drawing only approximately 6 milliwatts total. When operating transistors with such large collector and collector-to-base coupling resistances, it is necessary to carefully match transistors and resistors in the individual stages. The transistors were matched as closely as possible over a wide temperature range by actual comparison of characteristic curves under operating conditions using a transistor curve tracer. Resistor matching was accomplished by using 1% resistors throughout. The capacitors are not as critical and 5% tolerance was found to be satisfactory.

This circuit operates very reliably over a temperature range of $-15^{o}C$ to $+65^{o}C$ and a supply voltage range of 1.5 volts to 10 volts, which was the maximum test voltage used. The nominal operating voltage is approximately 6 volts.

Reset of the ten-stage scalers was required as discussed in the general description of the system operation. Reset is accomplished by removing the supply voltage from the left side of each stage. The switch shown in Figure 128 is actually a series transistor common to all ten stages. A reset pulse applied to the reset transistor base turns off the transistor and causes reset with all left-hand binary stage transistors conducting after reset.

Symmetrical triggering is used during normal operation with a negative trigger through isolation diodes to the "on" transistor base.

5. Clock

The main function of the electronic clock is to provide a time base for timing and switching operations in the system.

A 512 cps electromechanical tuning fork-oscillator combination provides an output which is then divided down in frequency by eight binary stages to 2 cps. This 2 cps output is used after further shaping and current amplification to drive the sensor commutator and other switches through pulsing of a Ledex rotary solenoid in this system. Other outputs are also taken from the clock binary chain as will be discussed later.

The main requirement on the clock is that its frequency remain quite constant over a wide range of temperature and a 20% range of supply voltage. The tuning fork is the most critical component. A hermetically sealed tuning fork was used.

The binary stages used in the clock are identical to those used in the ten stage scalers.

Included in the clock circuitry is a monostable multivibrator which generates a pulse of approximately 15 milliseconds duration (switch drive pulse of Figure 129) to control the switch drive in the system.

6. Switch Drive

The switch drive pulses from the monostable multivibrator in the clock are current amplified by the amplifier of Figure 130 to operate a Ledex rotary solenoid. The input pulses shown in Figure 130 have a maximum duration of 15 milliseconds and occur at a rate of two pulses per second.

The Ledex drive current is supplied by the only germanium transistor in the system. Because of the limited supply voltage a low saturation resistance transistor is required to assure sufficient current to drive the Ledex. At high temperature it is necessary to back-bias the H-7 base to reduce the collector current to a value below the release current of the Ledex rotary solenoid and also to reduce the power consumption during the time between drive pulses. In this system complications introduced in the solar battery supply ruled out the use of obtaining the necessary reverse bias by adding a mercury cell so that the base return was more positive than the emitter source. As indicated in Figure 130, reverse bias of the base of the H-7 between drive pulses is obtained by "base leak biasing". By proper adjustment of the time constant of the biasing circuit the H-7 is held cut off between pulses and sufficient base drive is supplied during the drive pulse.

In order to conserve power it is desirable to keep the duration of the drive pulse at a minimum consistent with reliable operation of the Ledex. It was found that the required duration of the drive pulse varied with supply voltage and temperature. A duration with enough margin of safety resulted in excessive power drain under normally expected conditions. A rather simple solution to this problem was to cause the Ledex to turn itself off. This was accomplished by mounting a moving contact on the Ledex itself. When this contact is closed by motion of the Ledex the monostable from which the drive pulse is obtained is pulsed off and shuts off the drive pulse. Ledex drive power requirements are further reduced by the use of the shunting diode. When the H-7 cuts off, the stored energy in the magnetic field of the Ledex produces a current in the same direction as the drive current during the collapse of the field. This continuing current aids in the completion of the rotary motion of the solenoid. The diode also eliminates the large negative voltage pulse that would occur when the field collapses and thus protects the H-7 from excessive collector voltage.

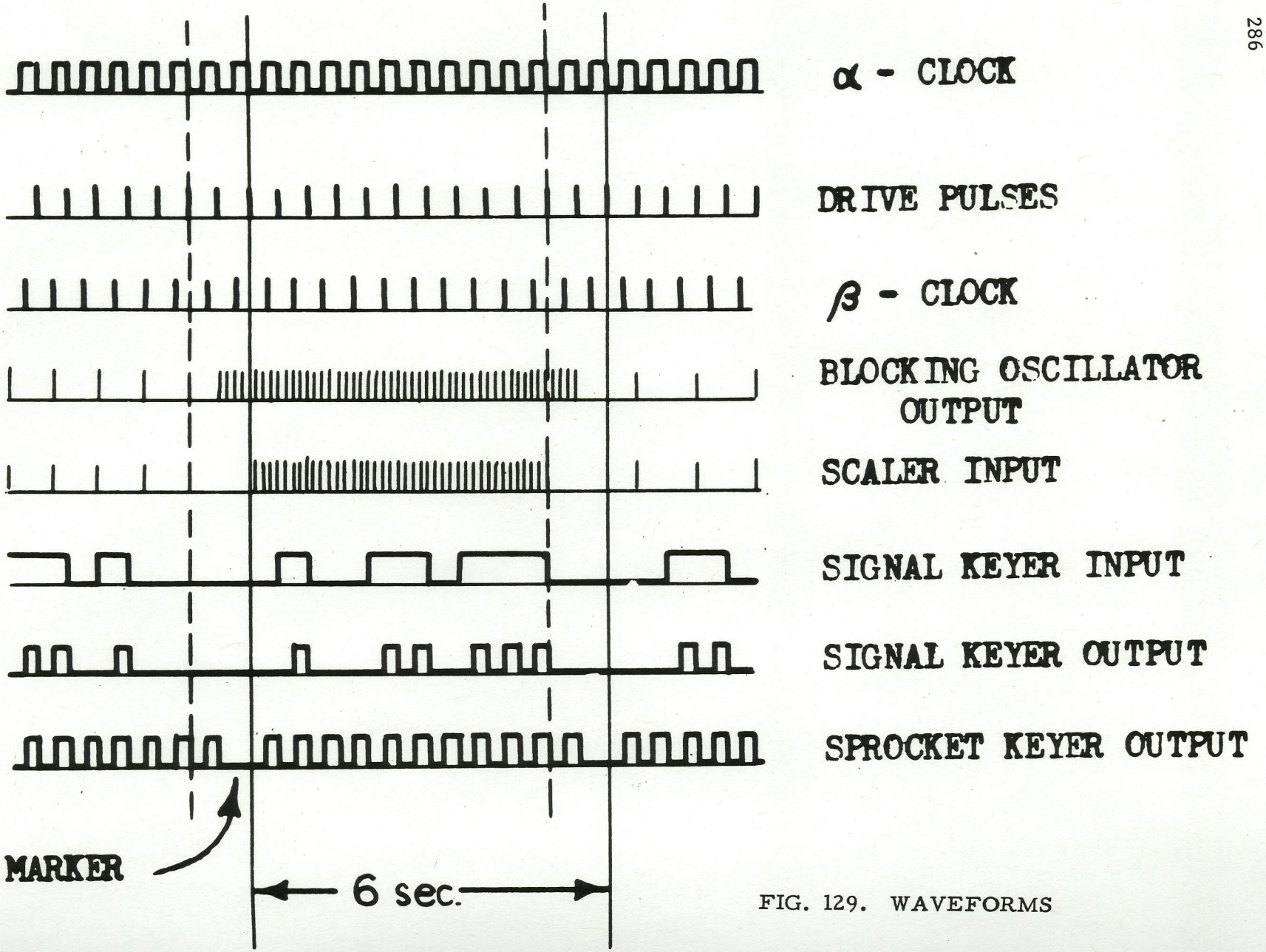

FIG. 129. WAVEFORMS

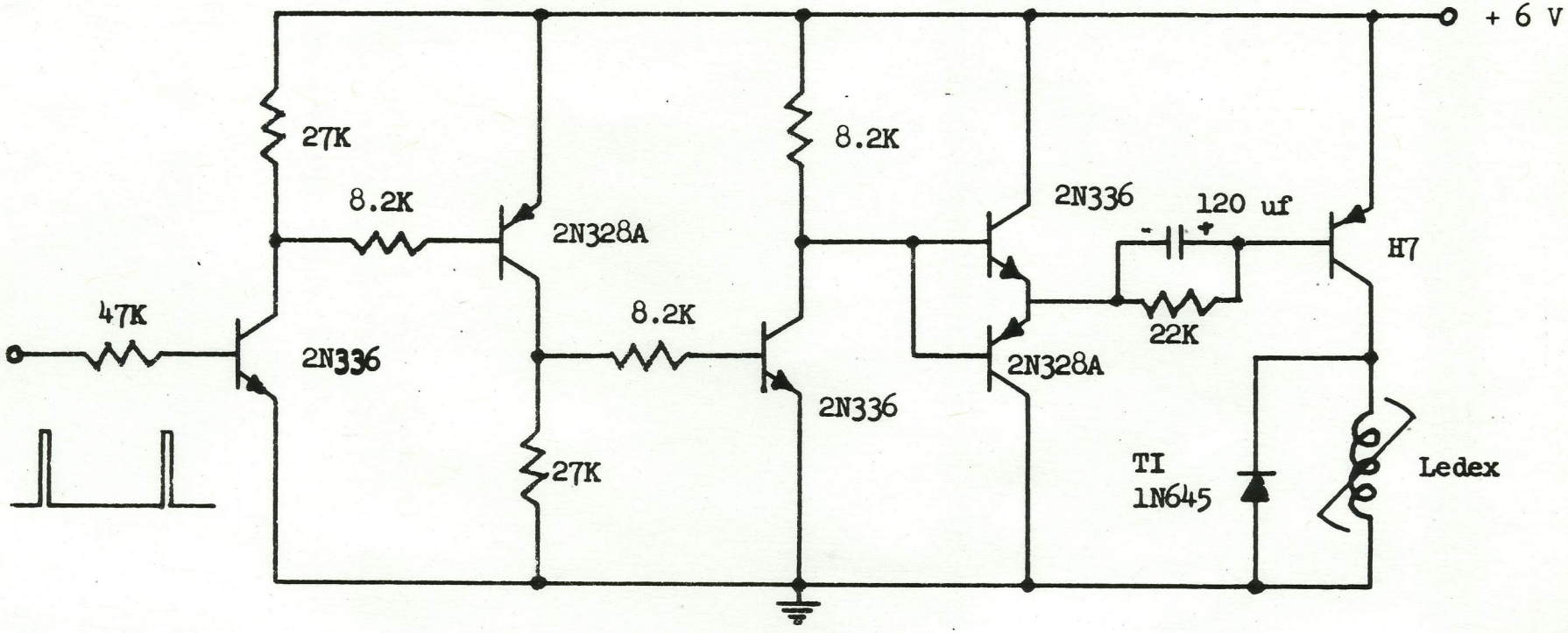

FIG. 130. LEDEX SOLENOID DRIVE CIRCUIT

The reduced duty cycle obtained by driving the Ledex with a minimum width pulse reduces the power required to mechanically drive the switches to about 40-45 milliwatts.

7. Switches

The switches operate as shown schematically in Figure 126.

8. Sprocket and Signal Keyers

The sprocket keyer output signal of Figure 129 is the α-clock pulse amplified except for the removal of every twelfth pulse. The removal of every twelfth pulse is accomplished by shorting out the α-clock pulse input under the control of the sprocket blank segment of S_2 of Figure 126. As previously explained, the blanked sprocket pulse indicates the beginning of a new number.

The signal keyer is an "and" or coincidence circuit. If both a sprocket and a "one" signal from a counter S_3 are present, the signal keyer produces an output. If either is missing, the output is zero. The output waveform is shown in Figure 129.

9. Subcarrier Oscillators

These oscillators convert the sprocket and signal pulses to frequency shift output. The sprocket subcarrier oscillator operates about a center frequency of 560 cps with a shift of approximately -6% when the sprocket keyer is off and +6% when it is on. The signal subcarrier oscillator operates similarly but with a center frequency of 730 cps. These two subcarriers are then combined with subcarriers from other experiments within the satellite to modulate the telemetering transmitter.

The system, in short, uses pulse code modulation of the subcarriers, which in turn modulate the main carrier.

The subcarrier oscillator assembly and transmitter were developed and supplied by the Army Ballistic Missile Agency, Huntsville, Alabama.

SECTION III. SYSTEM PERFORMANCE

The system design of the instrumentation described above has been directed toward production of extremely reliable systems capable of operating with minimum power drain with minimum size and weight and of transmitting intelligible signals over reasonably large distances. The small size and light weight have resulted from use of small components throughout. The system has been designed for reliability by providing parallel functions and fail-safe features wherever possible. For example, each sensor is sampled alternately by the two scalers because of the odd number of positions of S_1 and S_4 in Figure 126. Thus, failure of either scaler will not result in loss of information from any sensor. Dependable readings will occur half as often instead. Similarly all switch contacts are made in parallel on two separate switches so that breaking of any one wire or failure of any one switch contact will not produce loss of information.

Power consumption has been limited wherever possible by using care in the design of continuously operating circuits and by the intermittent operation of circuits whose power consumption is high. The figures presented in Table 11 show the power consumption. This power requirement is well within the capability of solar cells.

SECTION IV. DATA HANDLING AND TELEMETRY

The huge volume of data generated by the experiment described above dictates automatic data handling wherever possible. In a month's time, for example, 432,000 separate measurements will be transmitted.

It is obviously desirable to speed up the data for processing. The signal recorded on tape is in the form of a pair of audio tones each of which signals either "on" or "off". This recording is made at as slow a tape speed as possible in order to gain maximum compression of time scale. The resulting signal is discriminated and rerecorded (by pulse recording). It is then reproduced and recorded with speed-up at every stage until a tape is produced which, when played, will generate voltage levels which depend on original tone frequency and which are speeded up by a factor of 512. The pulse frequency is thus 1024 pulses per second.

The voltages so produced are used to turn on buffer circuits in a large digital computer. [1] The computer runs under control of a program which, at every sprocket pulse, checks to determine presence of a corresponding signal pulse. Such presence means a "1" was transmitted by

---

[1] The computer being used is an IBM 704; the buffer circuits turn on sense lights in the machine.

the satellite; absence denotes transmission of a "0". The computer thus builds up binary numbers in its memory according to the pair of impressed voltages. These binary numbers are precisely the numbers which were originally generated in the satellite. The time needed to load one month's data in this way would be about 1.4 hours.

SECTION V. PRELIMINARY RESULTS

Explorer VII perigee altitude is 560 km. This means that normally it is definitely above the F_2 layer of the ionosphere during daylight hours and above the F layer during the nighttime hours. Since the transmitter on board Explorer VII operates at 19.995 mc the quality of the received signal has a marked diurnal variation. During nighttime hours useful signals can be received for 15 to 20 or more minutes. This implies an orbit arc up to 1/5 the distance around the earth. On the other hand during daylight hours, when the ionosphere is less transparent, useful signals are received only about 2/3 to 1/2 as long. As a result the global coverage is considerably better during the local nighttime hours.

Table 11
APPROXIMATE SATELLITE POWER CONSUMPTION

ELEMENT	OPERATING POWER CONSUMPTION (MILLIWATTS)	PERCENT DUTY CYCLE	AVERAGE POWER CONSUMPTION (MILLIWATTS)
Clock	9	100	9
Switch Drive	1440	3	43
Blocking Oscillator	1	100	1
2 Scalers	13.2	100	13.2
Keyers	2.3	100	2.3
Total Power Directly Attributable to Instrumentation System			68.5
Telemetering Transmitter	2000	100	2000
Total Power Associated with Experiment			2068.5

Performance of the telemetering system is summarized in Table 12. The effect of noise depends upon the type of modulation and the method of demodulation. For the sake of calculation of Table 12, very simple detectors are assumed.

TABLE 12

CALCULATION OF TELEMETERING
PERFORMANCE IN THE PRESENCE OF NOISE

Transmitter Power	0.600 watt
Transmitter Frequency	19.995 mc
Modulation Method	Frequency Shift Telemetering tone amplitude modulates the 20 mc.
Distance over which telemetering is calculated	1400 miles
Bandwidth at narrowest point in receiving and demodulating system	10 cps
Assumed Satellite Antenna gain	-3 db
Assumed Receiver Antenna gain	2.14 db*
Calculated S/N Ratio in receiver**	28.5 db
S/N for one error in 1000 bits	17.5 db
Margin of system over that level required for 99.9% accurate transmission***	14 db

* Maximum gain of quarter-wave dipole
** Receiver noise figure is assumed to be 3 db.
*** Calculations have assumed free propagation. Obviously this ignores considerable ionosphere losses.

Table 13 is an IBM 704 listing of the sensor temperatures for a better than average daylight pass. Table 14 is the sensor temperature listing for a typical nighttime pass; the black hemispheres B_1 and B_4, the black sphere B_6 and the gold hemisphere G_5 are cold and are out of range of the telemetry system. The white hemisphere W_2 (actually more absorbent than the black hemisphere in the long infrared) is operating normally.

These preliminary results calculated by hand are given for the nighttime case for two reasons: (1) there is better global coverage and (2) the calculations are much simpler because only long wave radiation is being considered.

The energy balance equation for a spinning mirror backed hemisphere in space on the nighttime side of the earth reduces to

$$(2) \qquad \alpha \beta R\uparrow = 4 \pi \epsilon \sigma T_{W_2}^4 + 2H \frac{\partial T}{\partial t} - 2K (T_M - T_{W_2})$$

$$(3) \qquad R\uparrow = \frac{1}{\beta} \left[\frac{4 \pi \epsilon \sigma}{\alpha} T_{W_2}^4 + \frac{2H}{\alpha} \frac{\partial T}{\partial t} - \frac{2K}{\alpha} (T_M - T_{W_2}) \right]$$

where β is the solid angle to the earth, α and ϵ are the infrared absorptivity and emissivity respectively, σ the Stefan-Boltzman constant, H the heat capacity of the sensor and K is the conductivity between the sensor and mount, i.e. the mirror temperature, T_M.

Since $\alpha = \epsilon$ from Kirchoff's law, the value of the first term in equation (3), the greatest of the three, is determined by the absolute value of the temperature. A most pessimistic value of the error would place it at $\pm 1\,^{\circ}C$; a more likely value would be about one fourth of that. Even so, an error of $1\,^{\circ}C$. would give rise to an error of only 2.5% in the final value of $R\uparrow$. The satellite altitude and therefore the solid angle β is accurately known. At equilibrium the second term goes to zero, and finally it takes an error of 100% in the conduction term to give an error of 10% in the final result.

The sensor hemisphere coatings are special black and white paints selected for stability. Even so one cannot be certain that the coatings have not deteriorated in the vacuum of space where strong ultraviolet, X-ray and trapped radiation exists. In addition there is a possibility that absorptivity and emissivity obtained during calibration may not be constant with time. Fortunately, as can be seen from inspection of equation (3), large changes in ϵ (and therefore α for the same wavelength) have only a second order effect on the final values of radiation. These remarks are made not because there is any evidence of significant changes in emissivity after 8 months in orbit, but merely to establish confidence in the measurements.

The long wave radiation loss measured at night with the satellite is shown for two days in December 1959 and April 4, 1960 in Figures 131 to 133. Each dot along the orbit path is one observation. The map cannot be given a specific synoptic time because each pass along the orbit path is 101 minutes from the previous one. Thus, times on opposite sides of the map are 12 hours different. Because the orbit is inclined 51° to the equator, local time does not change with longitude as it does on a typical synoptic chart but instead it is a function of latitude. In the December series the satellite came out of the sun at the northern portion of the orbit belt and entered into the sunlight zone in the southern hemisphere. In the April series the reverse is true. The reader is reminded that in principal, only one point on the satellite map is synchronous in time with the 500 mb synoptic maps (Figures 134, 135 and 136) and the surface analysis map (Figure 137). The surface and 500 mb weather maps were chosen to have the best time fit with the satellite over the United States. The 500 mb and surface map analyses are obtained from the USWB Northern Hemisphere maps. Dotted lines are isotherms. By using several surface maps it was possible to make the frontal positions included on the December maps synoptic with the satellite passage in the area.

The radius of coverage from the Explorer VII to the horizon is large, i.e. roughly 25° of equatorial latitude at perigee and 34° at apogee. However, half the power is received from an area whose radius of coverage is only 550 km at perigee and 1120 km at apogee.

Some remarks should be made about the radiation pattern analysis. As mentioned already each dot along the orbit path represents one observation. In middle latitudes where the telemetry contact is most reliable the analysis will be more or less consistent from analyst to analyst. On the other hand in the tropical Pacific where the telemetry coverage is not as good and the distance between orbits is great, the analysis is subject to a considerable amount of interpretation. The map of December 2 (Figure 131) is a case in point. The orbit path SE along the Gulf of California very definitely establishes a low in outgoing radiation as latitude 20°N. Similarly the orbit path just to the west of Hawaii definitely establishes another low at about 10°N. However, on the orbit between these two the data are not as complete and while it shows a trend toward a low value, one cannot be sure, as the map indicates, that this is in fact the same large scale low radiation area. There is a general eastward movement to the cell from map to map in agreement with the wind direction at high levels during this season.

TABLE 13.
IBM LISTING OF SENSOR TEMPERATURES FOR A BETTER THAN AVERAGE DAYLIGHT PASS

TAPE NUMBER	: 1832	RECORD NUMBER	: 3
DATE	: 4-10-60	TRACKING STATION CODE:	8
DAYS FROM LAUNCH	: 180	Z TIME	: 15-24-47
SENSOR TEMPERATURES:	-ABSOLUTE		

REFS	BLACK 1	WHITE 2	TABOR 3	BLACK 4	GOLD 5	BLACK 6
0.00	0.00	0.00	0.00	290.32	320.14	299.75
270.57	290.41	259.35	266.24	291.75	321.83	300.48
263.85	287.92	262.27	260.57	292.14	323.07	301.03
301.63	291.40	262.70	267.27	292.40	324.28	301.39
294.36	291.67	263.02	267.61	292.59	325.47	301.70
335.64	291.92	263.35	254.38	292.72	326.25	299.13
278.61	292.25	263.68	268.27	282.82	327.02	298.46
281.37	283.44	264.23	268.75	293.24	328.16	302.66
65.00	292.82	264.45	268.91	293.49	328.53	302.84
993.00	293.14	265.13	269.38	293.88	329.64	303.08
271.72	293.46	265.69	269.69	294.26	330.00	303.20
264.42	293.84	265.92	270.15	294.39	330.72	303.33
301.50	294.03	266.38	270.60	294.78	331.43	303.45
294.27	294.35	266.84	270.89	294.90	331.79	303.51

TABLE 13. (Cont'd)

338.57	294.60	266.96	271.18	289.59	329.27	303.57
279.05	294.85	267.31	271.47	295.42	332.83	303.69
282.49	294.98	267.31	271.61	295.54	332.83	303.75
64.00	295.17	267.54	271.89	295.61	333.51	303.75
992.00	295.17	267.78	270.89	295.67	333.51	303.69
273.40	295.17	267.66	272.17	295.54	334.19	303.86
266.44	295.10	267.54	272.17	293.61	334.19	303.04
301.29	295.23	267.66	272.17	295.67	334.85	300.30
294.19	293.27	267.19	272.17	252.03	335.18	304.22
311.23	294.47	267.89	272.58	296.12	335.18	304.46
279.92	295.73	268.01	272.72	296.37	335.51	304.64
283.48	296.05	268.61	272.99	296.69	336.15	304.70
65.00	296.30	268.85	273.12	275.66	336.48	299.07
992.00	276.68	268.73	273.65	283.90	336.79	300.30
252.06	-277.37	-180.27	-246.24	-280.14	-334.19	-0.00
-239.34	0.00	0.00	0.00	0.00	0.00	0.00
0.00	0.00	0.00	0.00	0.00	0.00	0.00
0.00	0.00	0.00	0.00	0.00	0.00	0.00
0.00	0.00	0.00	0.00	0.00	0.00	0.00

Negative numbers indicate noise present.

TABLE 14.
SENSOR TEMPERATURE LISTING FOR A TYPICAL NIGHTTIME PASS

TAPE NUMBER	: 1823	RECORD NUMBER	: 3
DATE	: 4-7-60	TRACKING STATION CODE:	5
DAYS FROM LAUNCH	: 177	Z TIME	: 21-15-17
SENSOR TEMPERATURES:	- ABSOLUTE		

REFS	BLACK 1	WHITE 2	TABOR 3	BLACK 4	GOLD 5	BLACK 6
0.00	0.00	0.00	0.00	0.00	0.00	0.00
0.00	0.00	0.00	0.00	0.00	0.00	0.00
0.00	0.00	-206.04	258.25	0.00	0.00	244.20
986.00	0.00	203.89	257.30	0.00	0.00	242.08
270.73	0.00	202.16	256.32	0.00	0.00	0.00
258.45	0.00	200.30	255.57	0.00	0.00	0.00
297.09	-0.00	199.03	255.06	0.00	0.00	0.00
288.28	0.00	197.70	254.54	0.00	0.00	0.00
328.12	0.00	197.01	254.28	0.00	0.00	0.00
275.42	0.00	196.31	253.74	0.00	0.00	0.00
0.00	0.00	196.00	253.48	0.00	0.00	0.00
65.00	0.00	195.69	252.93	0.00	0.00	0.00
989.00	0.00	195.39	252.66	0.00	0.00	0.00
267.42	0.00	194.97	252.10	0.00	0.00	-0.00

TABLE 14. (Cont'd)

256.21	0.00	194.55	251.82	0.00	0.00	0.00
297.02	0.00	194.12	251.54	0.00	0.00	0.00
288.56	0.00	193.58	251.54	0.00	0.00	0.00
319.76	0.00	192.92	250.97	0.00	0.00	-0.00
271.94	0.00	192.81	250.68	0.00	0.00	0.00
0.00	0.00	192.26	250.39	0.00	0.00	0.00
64.00	0.00	192.14	250.10	0.00	0.00	0.00
982.00	0.00	191.80	-250.10	0.00	0.00	0.00
264.88	0.00	191.46	249.80	0.00	0.00	0.00
254.30	0.00	191.46	249.20	0.00	0.00	0.00
296.65	0.00	195.90	250.10	0.00	0.00	0.00
288.28	237.26	216.49	-252.10	-0.00	0.00	250.73
315.26	251.07	228.19	-254.01	-0.00	-0.00	-265.89
0.00	0.00	0.00	0.00	0.00	0.00	0.00
0.00	0.00	0.00	0.00	0.00	0.00	0.00
0.00	0.00	0.00	0.00	0.00	0.00	0.00

Negative numbers indicate noise present.

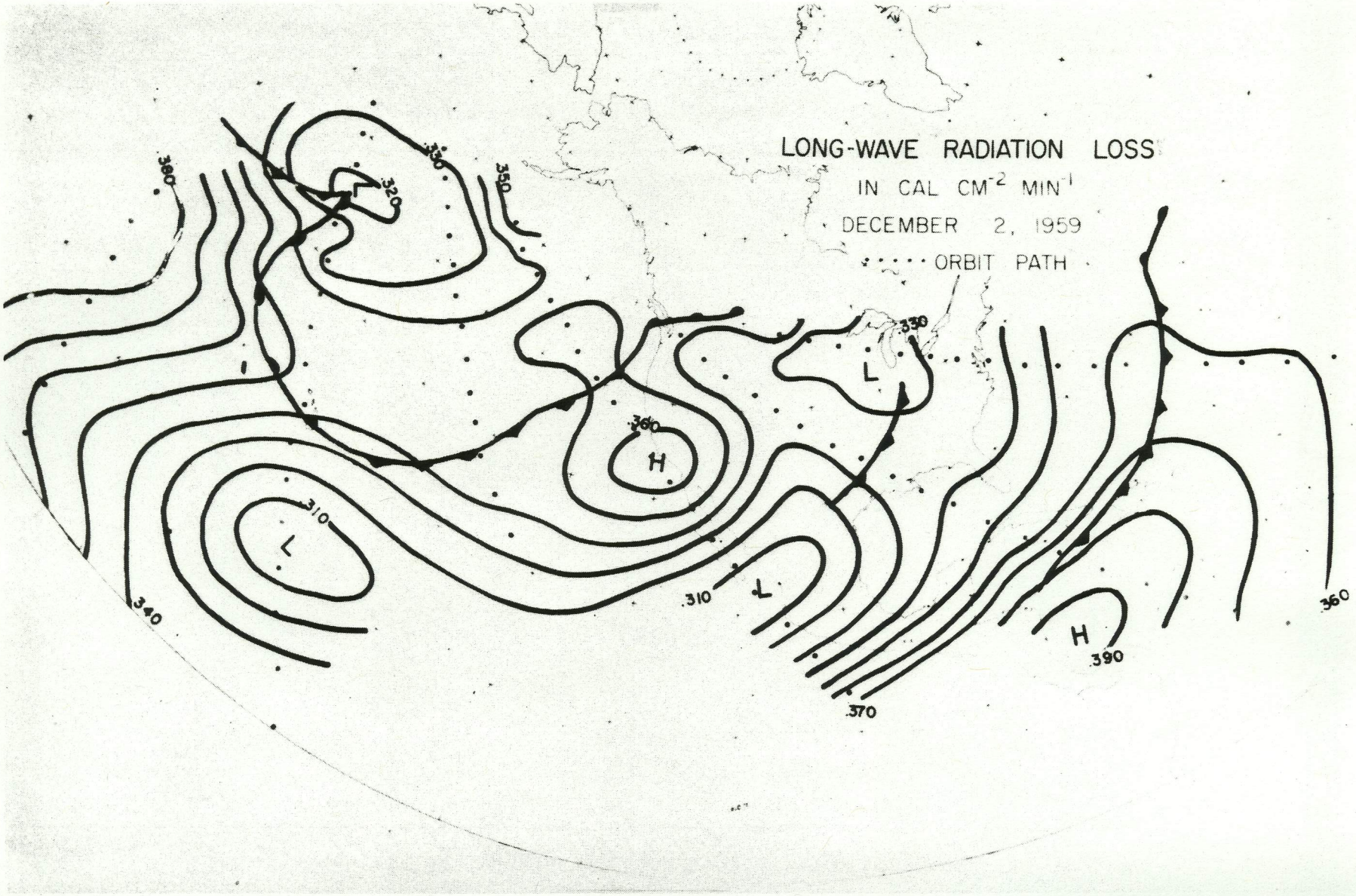
LONG-WAVE RADIATION LOSS
IN CAL CM^{-2} MIN^{-1}
DECEMBER 2, 1959
ORBIT PATH
360
330
320
350
L
330
360
H
310
L
340
310
L
360
H
390
370

FIG. 131.

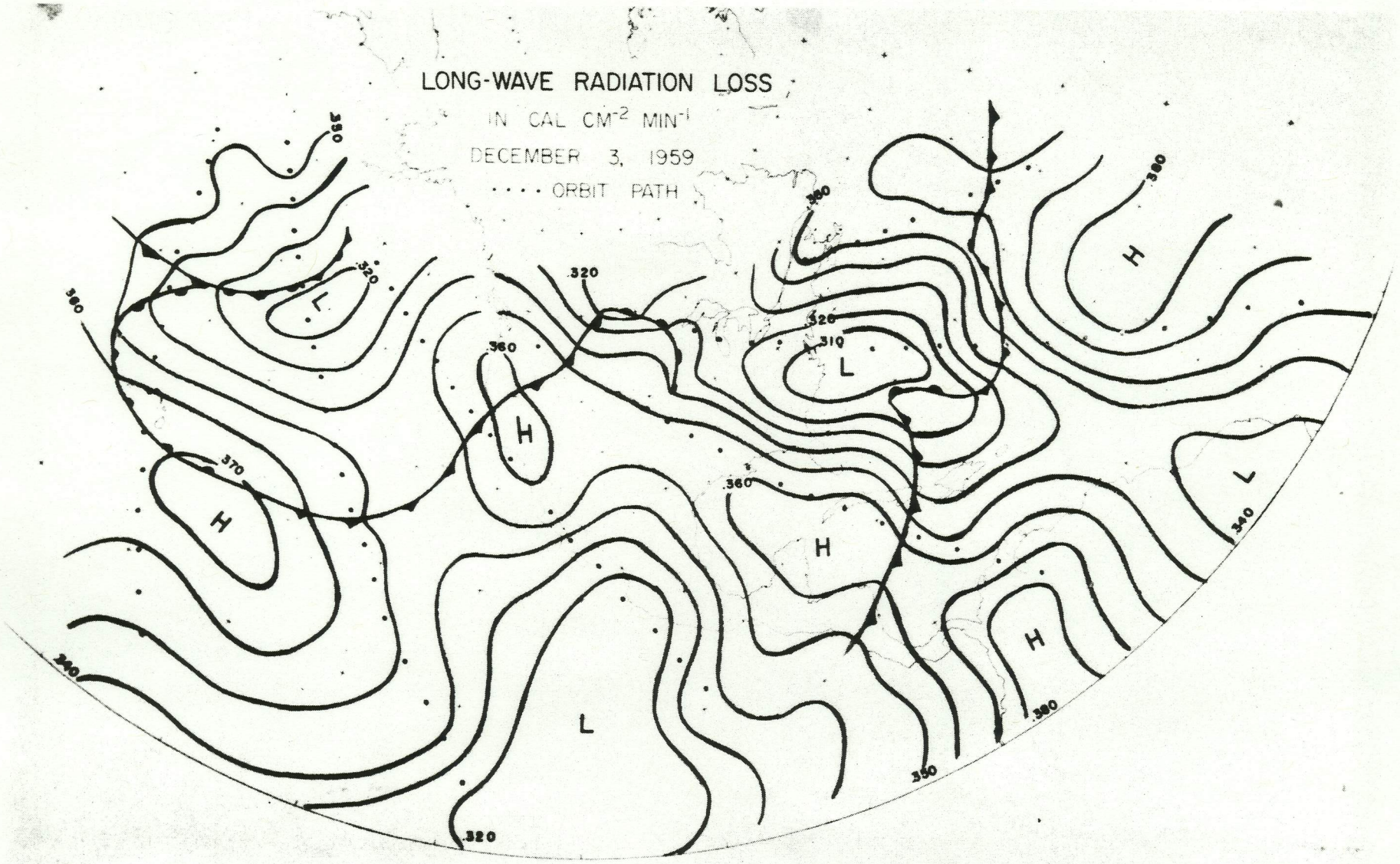
LONG-WAVE RADIATION LOSS
IN CAL CM^{-2} MIN^{-1}
DECEMBER 3, 1959
.... ORBIT PATH
H
L
350
320
360
370
340
310
380

FIG. 132.

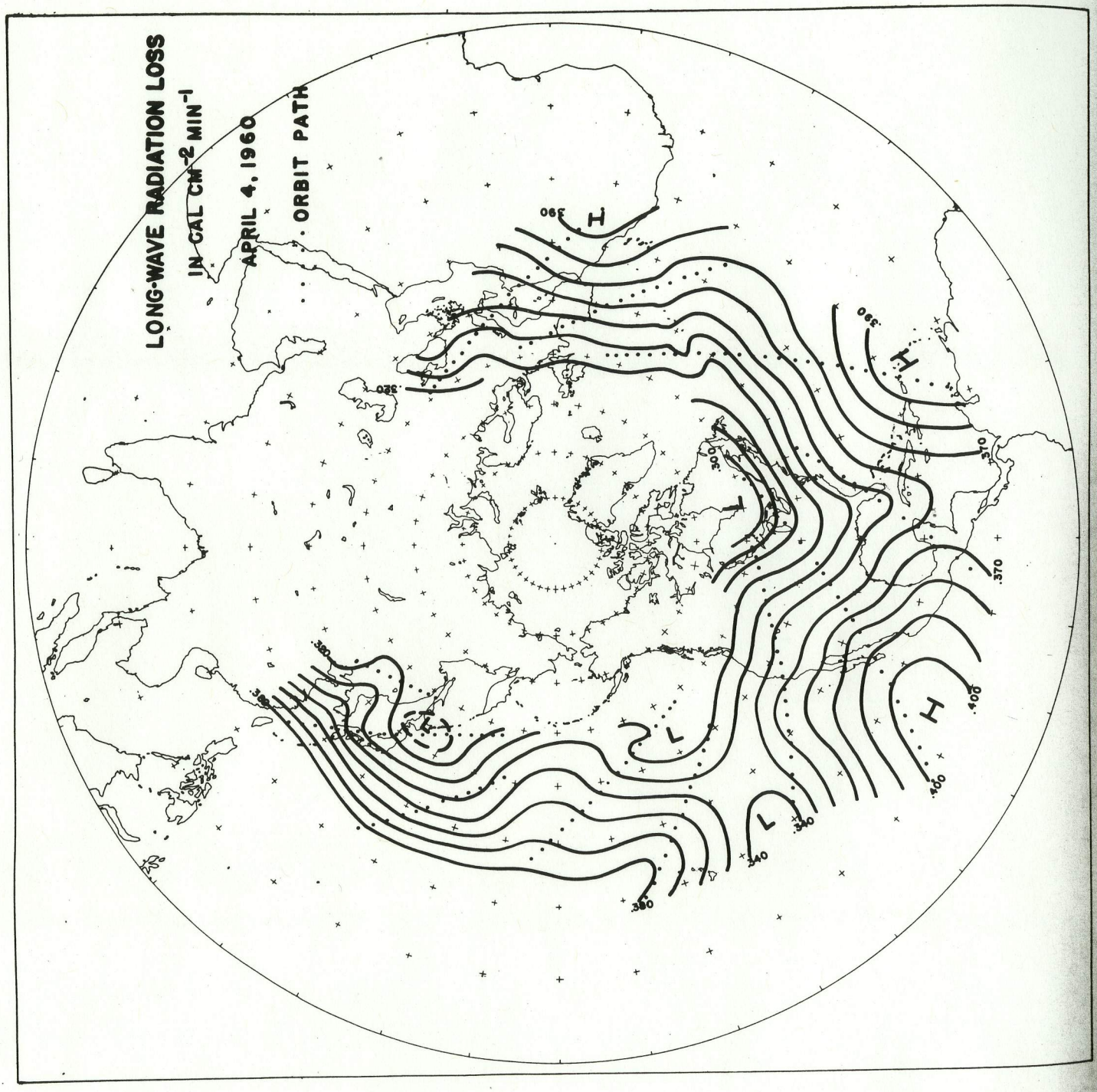
LONG-WAVE RADIATION LOSS
IN CAL CM^{-2} MIN^{-1}
APRIL 4, 1960
ORBIT PATH
H
L
390
380
370
360
350
340
330
320

FIG. 133.

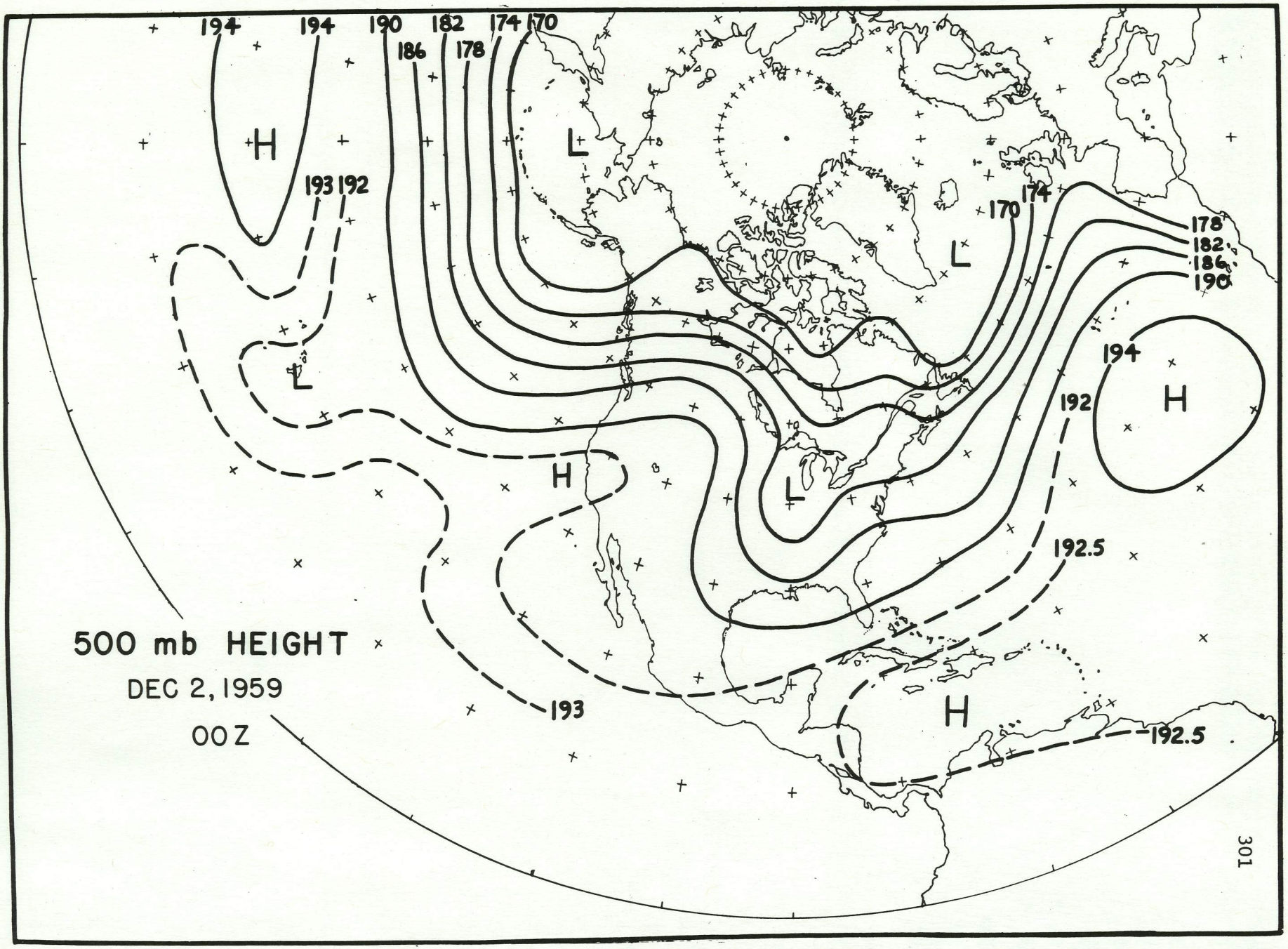
194
194
190
182
174
170
186
178
H
L
193
192
L
170
174
178
182
186
190
L
194
H
192
H
L
192.5
500 mb HEIGHT
DEC 2, 1959
00Z
193
H
192.5
301

FIG. 134.

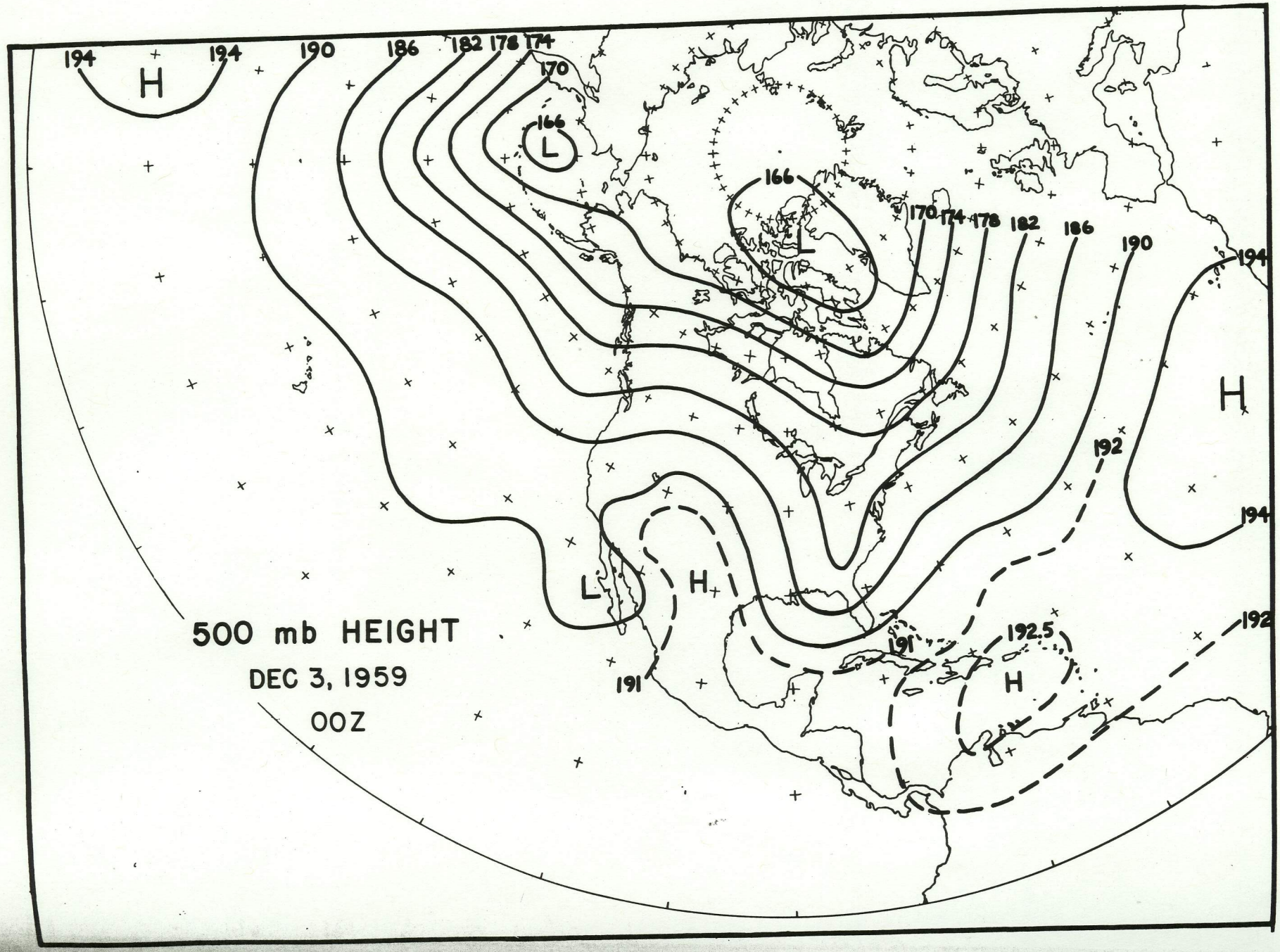
194
H
194
190
186
182
178
174
170
166
L
166
170
174
178
182
186
190
194
H
192
194
L
H
192.5
191
191
192
H
500 mb HEIGHT
DEC 3, 1959
00Z

FIG. 135.

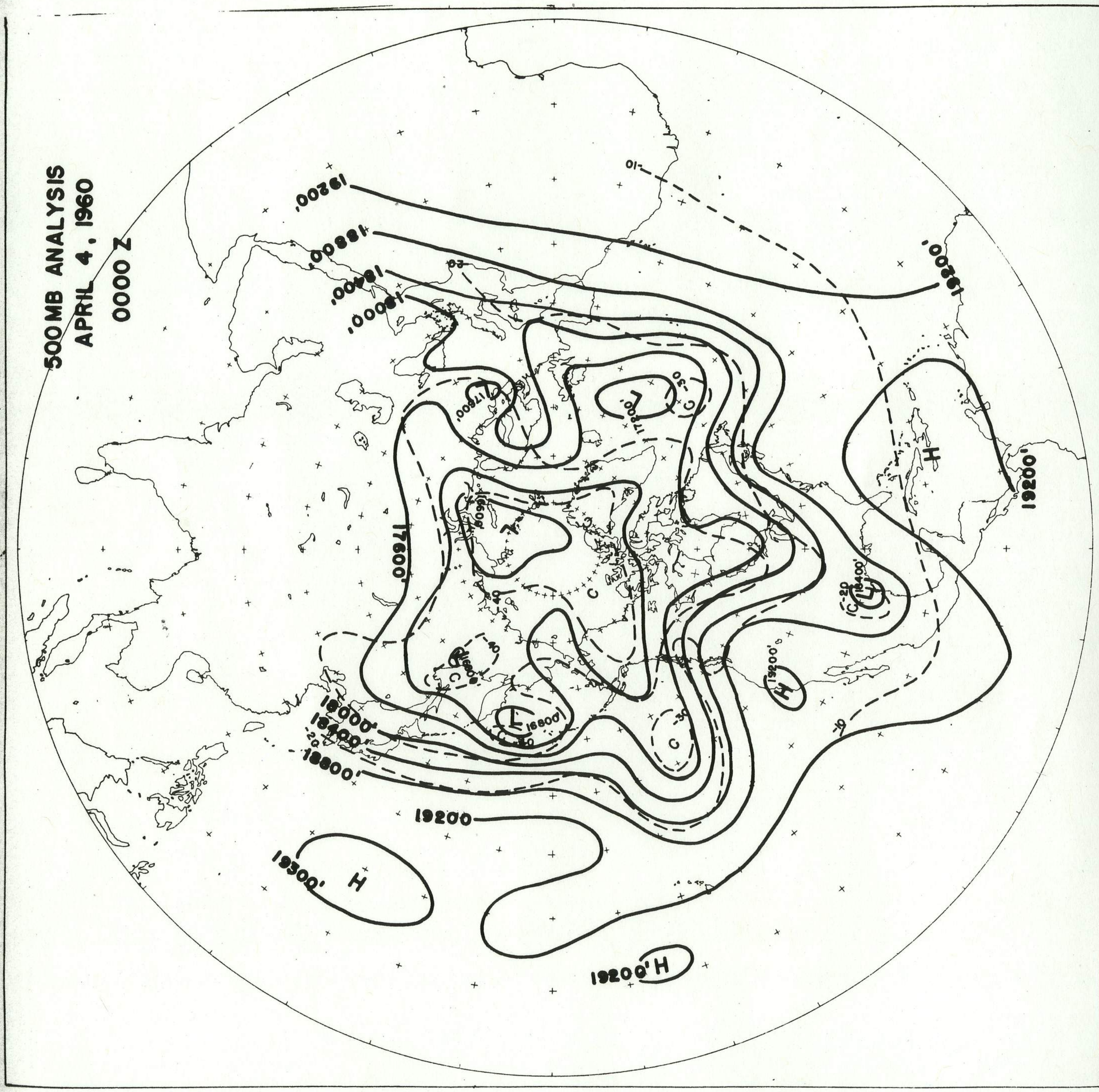

500MB ANALYSIS
APRIL 4, 1960
0000 Z
19200'
18800'
18400'
18000'
17600'
19300' H
19200' H
19200'

FIG. 136.

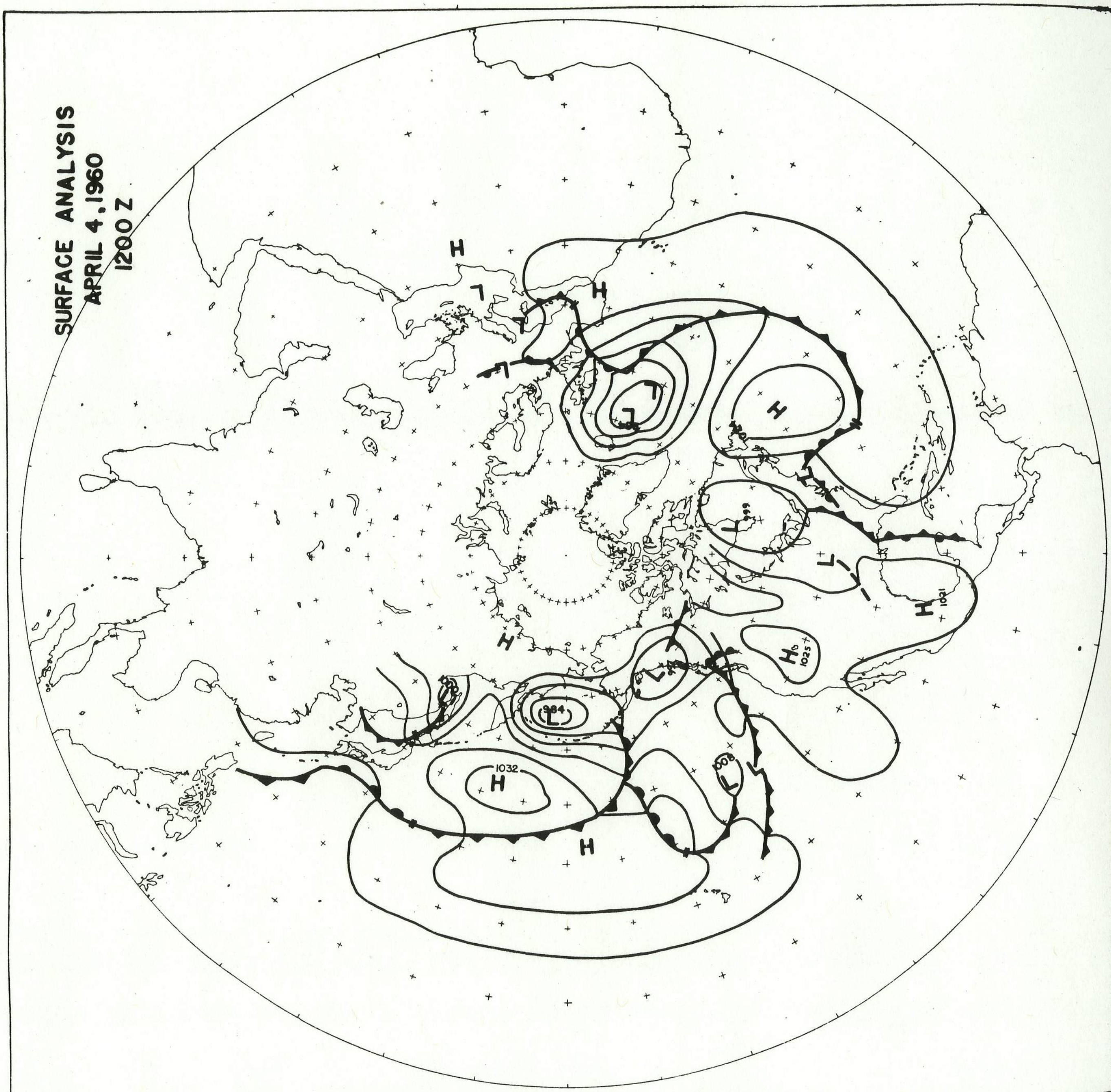

FIG. 137.

Despite the necessary shortcomings in the analysis there does seem to be a clear indication that large scale outward radiation flux patterns exist and that these patterns are related to the large scale features of the weather. Meteorologists expected a variation of outgoing radiation with latitude but the preliminary results show variation of the outgoing long wave radiation with longitude as well. Mossby's statement that the radiation loss is controlled by the circulation patterns is certainly verified. It is also apparent that these results re-emphasize the important role that clouds play in controlling the outgoing radiation. The accuracy of previous estimates of outgoing radiation will be governed to a large extent by the accuracy of the estimate of cloud cover.

It is of some interest to note that the radiation gradient with latitude for the April map is somewhat steeper than the latitudinal gradient for the December maps. Also the heat loss from the northern portion of the orbit belt is less in April than in December. The April radiation pattern looks more like a winter situation than the December map. An inspection of the 500-mb charts shows that this is as it should be. The north-south temperature gradient is tighter in the April case and the temperature at the northern border is significantly colder as well.

The writer wishes to emphasize that these charts represent only the beginning of an enormous amount of data. Also that here we have treated only one half of the problem, namely the radiation losses. Equally important to our understanding of the earth's heat budget are the gains from the sun. These will be treated in another paper.

It appears that very useful radiation data can be collected from a modestly instrumented earth satellite. Had Explorer VII carried a data storage unit so that the measurements for a complete orbit could be obtained by interrogation from a ground station, it would be possible to have maps, such as we have described, for the whole earth. The problem of analysis would not be more difficult because of the added data; it would be simpler. This is because most of the work now is involved with fitting many pieces of data into a comprehensive picture. We look forward to being able to do this in the near future.

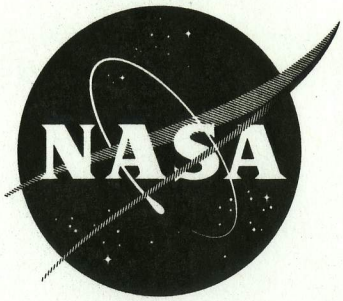

TECHNICAL NOTE
D-608

JUNO II SUMMARY PROJECT REPORT

Volume I

Explorer VII Satellite

George C. Marshall Space Flight Center
Huntsville, Alabama

NATIONAL AERONAUTICS AND SPACE ADMINISTRATION

WASHINGTON

July 1961